Distributions of Site-Hopping Geometries and Rates for Benzene Adsorbed on Ag–Y Zeolite

A. Gédéon,[†,§] D. E. Favre,[†] D. Reichert,[‡] J. MacNeil,[†] and B. F. Chmelka*,[‡]

Department of Chemical Engineering, University of California, Santa Barbara, California 93106, and Fachbereich Physik, Martin-Luther Universität Halle-Wittenberg, 06108 Halle, Germany

Received: March 18, 1999

Slow jump reorientation dynamics of benzene molecules adsorbed on Ag–Y zeolite (Si/Al = 2.4) have been investigated using solid-state nuclear magnetic resonance (NMR) spectroscopy. Multidimensional exchange ^{13}C NMR techniques establish that the benzene jump angle distribution is broad and that multiple benzene reorientation rates exist for site exchange among different local environments. Modeling of ^{2}H and ^{13}C NMR line shapes yields an apparent activation energy of 34 ± 2 kJ/mol and a preexponential factor of $k_0 = 2 \times 10^{10}$ s^{-1} ($\pm^1/_2$ decade) for the complicated molecular reorientation motions underlying benzene site-hopping dynamics in Ag–Y zeolite.

Introduction

The dynamics of guest molecules adsorbed within the cavities and channels of crystalline zeolite catalysts and adsorbents strongly depend on the structure and chemical composition of the zeolite, as well as on the molecular properties of the adsorbed species. A variety of host–guest interactions are possible, such as steric hindrance or an attractive interaction between an extraframework cation in the zeolite and the π-electrons of an adsorbed aromatic molecule.[1] These host–guest interactions affect the transport of adsorbed molecules; reported diffusion coefficients for molecules adsorbed in zeolites span 12 orders of magnitude, from 10^{-20} to 10^{-8} m^2/s, depending on the particular combination of zeolite structure, composition, temperature, and adsorbate guest.[2–4] Differences in adsorption and mass transport properties are exploited in separations processes and to alter selectivities in zeolite-catalyzed reactions.[5,6] However, the molecular origins of these macroscopic properties have generally been difficult to elucidate and are poorly understood. In this respect, the application of exchange NMR methodologies can provide new insight into the molecular origins of guest transport properties,[4,7,8] even in systems with appreciable disorder,[9] such as Ag–Y zeolite.

Silver-exchanged zeolites are useful catalysts for the epoxidation of ethylene, and these zeolites also have interesting electrical and optical properties.[10] Silver cations can exhibit unusually strong interactions (through participation of silver's d-electrons) with certain adsorbed species, such as ethylene or xenon (but apparently not benzene).[11,12] For example, ethylene adsorbs much more strongly on faujasite-type zeolites that are silver-exchanged compared to those that are calcium-exchanged.[11a] In contrast, the reverse situation applies for benzene, as evidenced by the more rapid reorientation dynamics of benzene on Ag–Y presented here, compared to benzene reorientation dynamics on Ca–LSX and Ca–Y zeolites.[4,7]
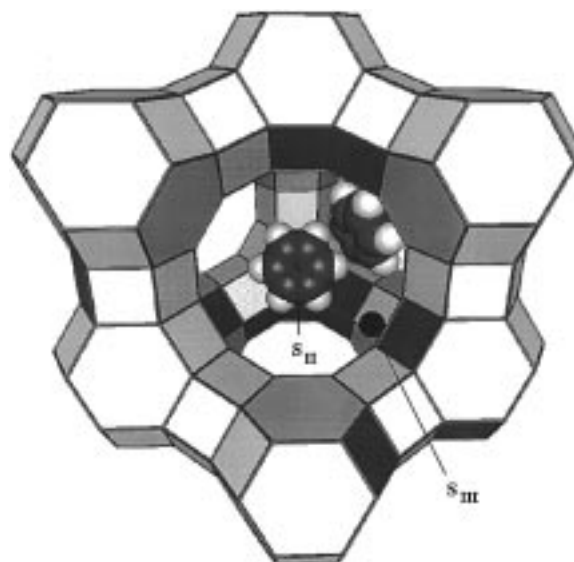

Figure 1. Schematic diagram of a single supercage cavity of Ag–Y zeolite containing benzene molecules adsorbed above an Ag$^+$ cation located at an SII cation site and at a window site. Additional adsorption sites may also exist in this system, such as at SIII cation positions, one of which is shown.

Because benzene interacts strongly with cations,[1] extraframework cations serve as the primary sites for benzene adsorbed on faujasite-type zeolites (compared to window sites, which are relatively unfavorable, see Figure 1).[13] Thus, the locations of Ag$^+$ cations are important factors to the present study of benzene reorientation geometries and dynamics on Ag–Y zeolite. Silver has been shown by X-ray diffraction to occupy SII sites within the supercage cavities,[14] as shown schematically in Figure 1. Additionally, ^{129}Xe NMR results imply that a small number of Ag$^+$ cations are located elsewhere in the supercage cavities.[12] While additional Ag$^+$ cations are not observed in Ag–Y supercage cavities by powder X-ray diffraction, there is evidence for cations at SIII sites in Ag–X.[14] Determining the location of the Ag$^+$ cations is made more difficult by the tendency of the silver species to form clusters in these systems, a process that can be mitigated by careful sample preparation to avoid

---

* To whom correspondence should be addressed.

† University of California.

‡ Martin-Luther Universität Halle-Wittenberg.

§ Permanent address: Laboratoire Chimie des Surfaces, Université Pierre et Marie Curie, CNRS-ESA 7069, 4, place Jussieu, 75252 Paris Cedex 05, France.

reduction of Ag^+ cations.[14,15] While the Ag^+ cations serve as the primary sites for benzene adsorption, less favorable sites exist in the 12-ring windows connecting adjacent supercage cavities.[13] A further complication is that adsorption of benzene can perturb the positions of the extraframework cations.[13b,16]

To assess the adsorption and transport properties of nanoporous solids, such as the benzene/Ag−Y system, a number of experimental techniques can be used to probe a wide range of complementary time scales. Incoherent quasi-elastic neutron scattering measurements probe rapid (10^{-12} to 10^{-8} s) molecular reorientation processes,[17] while the distortion of ^2H and ^{13}C NMR line shapes are sensitive to slower time scales, 10^{-6} to 10^{-4} and 10^{-5} to 10^{-3} s, respectively.[18] Muon spin resonance has recently been employed by Roduner and co-workers[19] to probe reorientation time scales of 10^{-8} to 10^{-7} s for radical species adsorbed on zeolites. Modeling various NMR relaxation processes, such as T_1, T_2, or $T_{1\rho}$, allows time scales from 10^{-10} to 10^{-4} s to be studied,[20] though the interpretation of the relaxation times and line shapes requires a model of the molecular motion that is generally nonunique.[18] To measure reorientation time scales and geometries in the ultraslow regime (10^{-3} to 10^2 s) directly, exchange NMR techniques have recently been adapted for zeolite/guest systems[4,7−9] and are applied here.

Two-dimensional (2D) exchange ^{13}C NMR and stimulated echo measurements[21] are used to quantify the distribution of reorientation geometries and slow ($>10^{-3}$ s) time scales for benzene jump reorientation processes occurring on Ag−Y zeolite at low temperature ($\leq$193 K). Reduced three- (3D) and four-dimensional (4D) NMR techniques provide additional details about the reorientation motions, including the relative rates of small-angle versus large-angle reorientation motions, as well as the rate exchange of benzene molecules within the observed reorientation rate distribution. At higher temperatures (253−353 K), modeling of ^{13}C magic-angle spinning (MAS) and ^2H NMR line shapes is used to characterize more rapid (10^{-5} to 10^{-3} s) reorientation dynamics. Benzene molecules adsorbed on Ag−Y zeolite participate in a diverse range of reorientation processes, which result in a broad distribution of site-hopping geometries and rates that can be quantified using these complementary techniques.

Experimental Section

Sample Preparation. Commercial Na−Y zeolite (Union Carbide LZY52, Si/Al = 2.4) was successively ion-exchanged three times in 1 M $Ag(NO_3)$ solution at room temperature, in the dark and under reflux conditions for 12 h using 25 mL of solution/g of hydrated zeolite. After each ion exchange, the solution was filtered, and the solid was washed 10 times with distilled water. The powder X-ray diffraction pattern of the Ag-exchanged powder showed that the material possessed the same faujasite structure as the initial Na−Y material, with no detectable features from impurity phases. The degree of silver ion-exchange was greater than 98%, as determined by elemental analysis. The ^{29}Si MAS NMR spectrum of Ag−Y product confirmed that the material had a Si/Al ratio of 2.4.

After the samples were dehydrated under vacuum ($<10^{-3}$ Pa) at room temperature, the samples were heated slowly (0.75 °C/min) to 573 K and exposed to oxygen gas at a pressure of 400 Torr. The samples were then slowly heated to 673 K and maintained at this temperature for 3 h under oxygen, after which they were evacuated ($<10^{-3}$ Pa) at 673 K for at least 12 h. The samples were then cooled to room temperature. The resulting zeolite samples were white, indicating the absence of reduced silver clusters.

A bulk loading of about two benzene molecules per supercage was subsequently introduced into each of the samples from bulbs that had been volumetrically loaded in a glovebox under a nitrogen atmosphere. The samples were then cooled with liquid nitrogen and flame-sealed in glass ampules, after which they were placed in an oven at 373 K for 12 h to distribute the benzene throughout each sample.[7b] One sample was loaded with perdeuterated benzene (^2H-enriched at all six hydrogen sites), and a second sample was loaded with benzene ^{13}C-enriched to 99% at a single ring site.[22] The use of isotopically labeled benzene, as opposed to ^2H and ^{13}C in natural abundance (0.015% and 1.1%, respectively), was necessary to ensure sufficient signal intensity to obtain NMR spectra within reasonable measurement times. For the case of ^{13}C, enrichment at a single ring site, instead of all six carbon sites, represents a compromise between further enhancement of the NMR signal intensity and undesirable broadening of ^{13}C NMR signals due to homonuclear $^{13}C-$ ^{13}C dipolar couplings.

NMR Experiments. All ^{13}C NMR experiments were performed on a Chemagnetics CMX-180 spectrometer operating at 45.3 MHz for ^{13}C and 180.1 MHz for ^1H. Magic-angle spinning (MAS) spectra were acquired using 7.5-mm diameter zirconia PENCIL rotors with the samples spinning at $\omega_R = 2\pi \times 1500$ Hz at temperatures between 185 and 366 K. The reported temperatures are corrected values based on calibrations with methanol ($<$311 K) and ethylene glycol ($>$ 311 K).[23] The spectra were recorded using high-power proton dipolar decoupling (DD) with the one-pulse sequence shown in Figure 2a. The ^{13}C $\pi/2$-pulse length was 4 μs, and recycle delays ranged from 10 to 20 s. For each spectrum, 1024 complex points were acquired with a dwell time of 30 μs.

Static two-dimensional (2D) exchange ^{13}C NMR spectra were recorded in off-resonance mode using a standard cross-polarization (CP) pulse sequence,[21,24] shown in Figure 2b. Transverse ^{13}C magnetization was created by cross-polarization from nearby protons and allowed to evolve under proton decoupling during the evolution time t_1. The ^{13}C magnetization was subsequently stored along the z-axis by a $\pi/2$-pulse, which initiated the mixing time t_m. Depending upon the phase of this first ^{13}C $\pi/2$-pulse, the amplitude of either the $\langle \cos(\omega_1 t_1)\rangle$ or $\langle \sin(\omega_1 t_1)\rangle$ component was stored. Molecular reorientation motions can take place during the mixing period, thereby altering the NMR frequencies. ^{13}C NMR signals were measured during the detection time t_2 under conditions of dipolar decoupling, following the second ^{13}C $\pi/2$-pulse, which restores ^{13}C magnetization to the transverse plane. A refocusing π-pulse was used to create a Hahn echo in the detection period, to overcome the dead time of the receiver. A stimulated echo occurs at the time $t_2 = t_1$. For the 2D exchange NMR experiment, a 2D data set $F(t_1,t_2;t_m)$ was generated by repeating the experiment with incremented values of the evolution time t_1 while keeping t_m constant. Fourier transformation with respect to the two times t_1 and t_2 yielded the two-dimensional exchange spectrum $S(\omega_1,\omega_2;t_m)$, which correlates the frequencies before and after the mixing time. A 32-scan phase cycle was used to suppress spectral artifacts, arising mainly from signal contributions created by spin−lattice relaxation during the mixing time. Spectra were acquired at temperatures of 163, 183, and 193 K. The $\pi/2$-pulse lengths for ^1H and ^{13}C ranged between 4.5 and 4.8 μs; CP contact times of 10−12 ms were used, and recycle delays varied from 6 s (193 K) to 15 s (163 K). A typical delay time between the two pulses of the Hahn echo sequence in the detection period was 70 μs. In the detection period, 128 complex points were acquired with a dwell time of 15 μs; 40 points in 30 μs increments were

Benzene Adsorbed on Ag−Y Zeolite

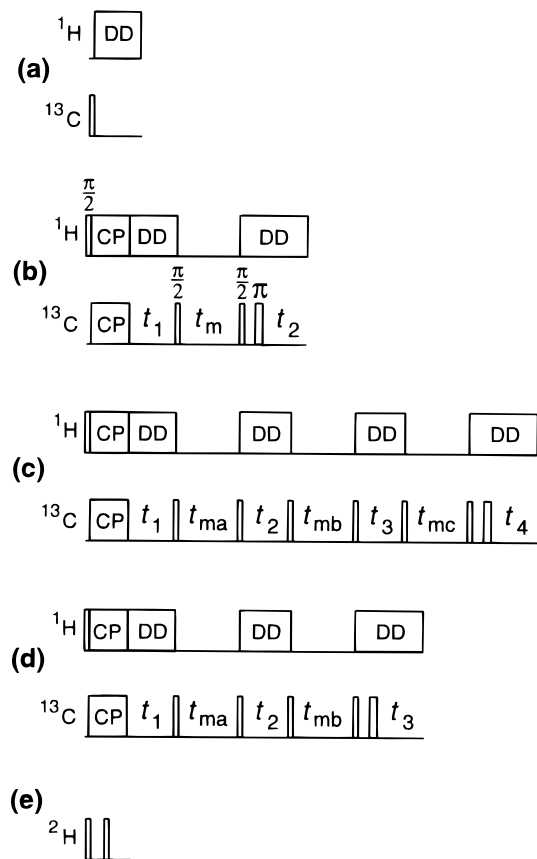*J. Phys. Chem. A, Vol. 103, No. 34, 1999* **6693**

Figure 2. Schematic representations of the radio frequency (rf) pulse sequences used in this study. (a) The one-pulse ^{13}C NMR experiment with high-power proton dipolar decoupling (DD) during acquisition. (b) The cross-polarization (CP) pulse sequence for two-dimensional (2D) exchange ^{13}C NMR and stimulated echo measurements. (c) The pulse sequence for reduced four-dimensional (4D) echo ^{13}C NMR measurements. The NMR signal surviving the first stimulated echo at $t_2 = t_1$ undergoes a second stimulated echo at time $t_4 = t_3$. (d) The pulse sequence for the three-dimensional (3D) DICO ^{13}C NMR experiment. Two-dimensional data sets are generated by incrementing the times t_1 and t_2 simultaneously, while keeping t_{ma} and t_{mb} constant. (e) Solid-echo sequence for on-resonance acquisition of ^{2}H NMR spectra.

measured in the evolution period. Prior to Fourier transformation, the data array was zero-filled to dimensions ($\omega_1 \times \omega_2$) = 256×512 and Gaussian damping of 800 Hz was applied in both dimensions. The final spectrum, with a spectral width of $2\pi \times 16.7$ kHz in both dimensions, was obtained by cutting the 2D array to dimensions 128×128 and discarding the $^7/_8$ of the 2D Fourier transform that contains either only baseline (ω_2) or the completely equivalent spectrum in the ω_1 dimension.

The time-domain signals for the 2D exchange ^{13}C NMR spectra acquired in off-resonance mode at $T = 193$ K contain stimulated echoes that provide information on molecular reorientation geometries. Time-domain stimulated echo signals were also acquired on-resonance at $\omega_{iso} = 126$ ppm at $T = 193$ K and using the pulse sequence shown in Figure 2b. To characterize time scales (or rates) for large-angle molecular reorientation motions (see below), $t_1 = t_2 = 150$ μs was held fixed and the mixing time t_m was varied. As a probe of the molecular reorientation rate distribution (see below), reduced 4D echo signals were acquired using the pulse sequence shown in Figure 2c, with $t_1 = t_2 = t_3 = t_4 = 150$ μs held fixed, the mixing times $t_{ma} = t_{mc}$ set to 220 ms, and t_{mb} varied. In the reduced 4D echo pulse sequence, a Hahn echo was used to overcome the dead time of the receiver. To complement the

extraction of reorientation time scales from static 2D exchange spectra, on-resonance stimulated echoes with $t_1 = t_2 = 50$ μs were acquired at temperatures of 153, 163, 173, 183, and 193 K. All ^{13}C echo data were corrected for T_1 relaxation, which varied between 12 s (193 K) and 17 s (153 K).

Static three-dimensional (3D) *DI*fference *CO*rrelated exchange spectroscopy[25] ^{13}C NMR spectra were recorded in on-resonance mode using the pulse sequence shown in Figure 2d. DICO ^{13}C NMR spectra were acquired at a temperature of 193 K, with a first mixing time $t_{ma} = 1000$ ms and second mixing times $t_{mb} = 1, 10, 100,$ and 500 ms. The $\pi/2$-pulse lengths for ^{1}H and ^{13}C were 4.5 and 4.8 μs, the CP contact time was 10 ms, and the recycle delay was 6 s. Two separate time-domain signals were acquired, each with a 32-scan phase cycle given in ref 26. Fourier transformation and addition of the signals resulted in a 2D spectrum $S(\omega_d,\omega_3;t_{ma},t_{mb})$ that is equivalent to a projection of a 3D exchange spectrum. A Hahn echo was used to overcome the dead time of the receiver, with a typical delay time between the two pulses of 108 μs. In the detection period, 64 complex points were acquired with a dwell time of 50 μs; 35 points in 50 μs increments were measured in the evolution period. Prior to Fourier transformation, both data arrays were zero-filled to dimensions ω_d ($=\omega_1 - \omega_2$) $\times \omega_3 = 128 \times 128$. The two data sets were combined to yield a 2D projection of a 3D spectrum with a spectral width of $2\pi \times 20$ kHz in both the ω_d and ω_3 dimensions.

Static ^{2}H NMR spectra were acquired using the solid-echo pulse sequence shown in Figure 2e to overcome the dead time of the spectrometer receiver. Measurements were performed on a Chemagnetics CMX-500 spectrometer operating at 76.5 MHz for ^{2}H, at temperatures between 293 and 368 K. A ^{2}H $\pi/2$-pulse length of 3.1 μs and a pre-echo delay of 50 μs were used. Recycle delays varied from 3 to 4 s. Normally 128 complex points with a dwell time of 6 μs were acquired.

Theory and Methods

A brief introduction to the NMR experiments used in this study is provided below. For more background on these techniques, the reader is referred to NMR texts, such as refs 21 and 24.

Orientation Dependence of Anisotropic NMR Frequencies. In the solid state, NMR frequencies depend on the orientations of molecules or molecular segments relative to the external magnetic field $\mathbf{B}_0$, due to the anisotropy of the nuclear spin interactions. These orientation-dependent interactions are described by second-rank tensors. For the case of a spin $I = {}^1/_2$ nucleus, such as ^{13}C, the anisotropy of the chemical shift interaction leads to an angular dependence of the NMR frequency given by

$$\omega'(\alpha,\beta) = \omega_{iso} + \frac{\delta}{2}(3\cos^2\beta - 1 - \eta\sin^2\beta\cos(2\alpha)) \quad (1)$$

where ω_{iso} denotes the Larmor frequency including the isotropic chemical shift, δ specifies the coupling strength, and the asymmetry parameter η represents the deviation from axial symmetry about the z-axis of the coupling tensor $\boldsymbol{\sigma}$. The polar angles α and β describe the orientation of the magnetic field $\mathbf{B}_0$ in the principal axes system of the interaction tensor $\boldsymbol{\sigma}$. The principal axes system for the generally dominating intramolecular interactions is determined by the local symmetry of the molecule in the vicinity of the nucleus under study. In the C_6H_6/Ag−Y system, benzene molecules spin rapidly about their 6-fold axes, anisotropically averaging the chemical shift tensor of each molecule and yielding a ^{13}C spectrum with $\eta = 0$. Therefore, only the angle β between the z-principal axis of the

chemical shift tensor (directed, in the case of benzene, along the 6-fold symmetry axis of the molecule perpendicular to the ring plane) and the external magnetic field is relevant:

$$\omega'(\beta) - \omega_{iso} = \omega = \frac{\delta}{2}(3\cos^2\beta - 1) = \delta P_2(\cos\beta) \quad (2)$$

where $P_2(\cos\beta)$ is the second Legendre polynomial. In ^{2}H NMR ($I = 1$) the dominant interaction is between the electric field gradient and the nuclear electric quadrupole moment. The angular dependence of the ^{2}H NMR frequency has the same form as eqs 1 and 2, except for a "±" sign in front of the angular-dependent term, which accounts for the two transitions of the spin $I = 1$ system.

Two-Dimensional Exchange NMR. Two-dimensional exchange NMR[21,24] monitors changes in angular-dependent NMR frequencies occurring on a time scale ranging from milliseconds to a few seconds. This is achieved by monitoring frequencies before and after a so-called mixing time, during which spin exchange and/or molecular reorientation motions can occur. In practice, this is achieved by correlating the frequencies in the evolution (t_1) and detection (t_2) periods, which bracket the mixing time (t_m) as shown schematically in Figure 2b. For characteristic time scales on the order of the mixing time for the process causing such frequency changes, and with the condition that $t_m \gg t_1, t_2$, NMR frequencies can be considered constant during the evolution and detection periods. Changes in the NMR frequencies manifest themselves as off-diagonal intensity in a 2D exchange spectrum $S(\omega_1,\omega_2;t_m)$, which can be regarded as a correlation map of the frequencies measured in the evolution and detection periods, ω_1 and ω_2, respectively, and which parametrically depends on the mixing time t_m. The two-dimensional spectrum $S(\omega_1,\omega_2;t_m)$ represents a direct mapping of the joint probability density of finding a benzene molecule in a certain orientation with respect to the external magnetic field, and thus with a certain NMR frequency ω_1 during the evolution period t_1, and after a time interval t_m later, finding the same benzene molecule with an NMR frequency ω_2 during the detection period t_2. If NMR frequencies change on a time scale comparable to t_1 or t_2 (in practice, faster than ca. 1 ms), frequencies can no longer be considered constant during the evolution and detection periods and analysis of the data becomes more involved.[27] The upper limit for the mixing time t_m is established by spin−lattice relaxation, which causes the magnetization to decay to equilibrium with a time constant T_1 that is typically on the order of several seconds in ^{13}C NMR.

Figure 3 displays 2D exchange ^{13}C NMR spectra acquired at 193 K for benzene adsorbed on Ag−Y zeolite, showing an inhomogeneously broadened line shape that reflects an isotropic distribution of benzene molecular orientations. In Figure 3a all spectral intensity is confined to the diagonal ($\omega_1 = \omega_2$) of the 2D plane, indicating that NMR frequencies have not changed during the course of the $t_m = 1$ ms mixing time, and consequently affirming that no detectable molecular hopping or spin exchange has occurred among different adsorption sites on this time scale. The situation is considerably different for the spectrum in Figure 3b, which was acquired under identical conditions, except for the use of a longer mixing time ($t_m = 4000$ ms). The spectrum in Figure 3b displays significant off-diagonal intensity due to ^{13}C NMR frequency changes. If the distribution of reorientation angles β_3 (the angles between the relative orientations β_1 and β_2 of adsorbed molecules during t_1 and t_2, respectively) was narrow, a well-defined elliptical ridge pattern (see Figure 6a) would be present in the 2D exchange spectrum.[7,21,28] The absence of such a narrow elliptical ridge in
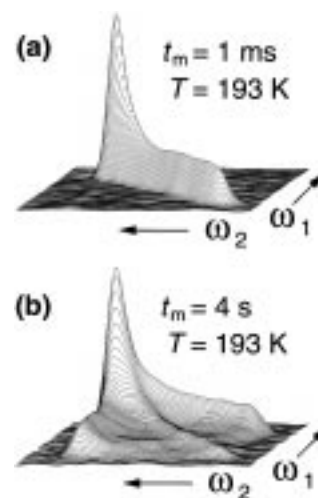

Figure 3. Experimental 2D exchange ^{13}C NMR spectra for a bulk loading of two adsorbed benzene molecules per Ag−Y zeolite supercage, acquired at $T = 193$ K using the pulse sequence shown in Figure 2b with different mixing times t_m. (a) $t_m = 1$ ms: intensity exclusively along the spectrum diagonal ($\omega_1 = \omega_2$) indicates that no detectable exchange of benzene molecules among adsorption sites occurs on this time scale. (b) $t_m = 4$ s: off-diagonal intensity indicates that orientation-dependent ^{13}C NMR frequencies change on this time scale. The lack of a distinct elliptical feature indicates that the molecular reorientation geometry among adsorption sites includes a broad distribution of angles. The spectra have been cut to $2\pi \times 12.5$ kHz in both dimensions.
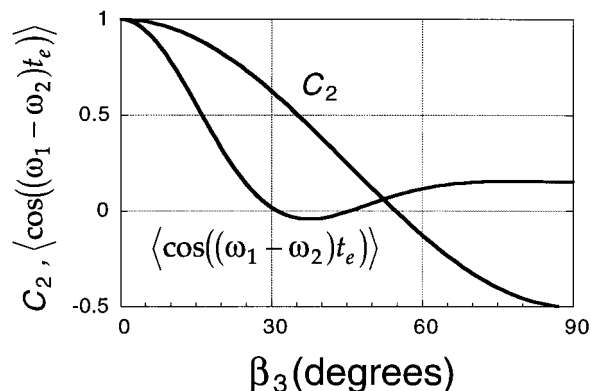

Figure 4. Simulated ^{13}C NMR stimulated echo intensity and the C_2 correlation function calculated as functions of the molecular reorientation angle β_3, for a ^{13}C chemical shift tensor corresponding to $\omega_{iso} = 126$ ppm, $\delta = -122$ ppm ($= -5.53$ kHz at 4.2 T), and $\eta = 0$. The stimulated echoes intensities were calculated numerically for on-resonance acquisition with $t_e = 150$ μs. For C_2, the zero of the ω_1 and ω_2 frequency axes is ω_{iso}, resulting in $C_2 = \langle P_2(\cos\beta_3)\rangle$, where P_2 is the second Legendre polynomial.

Figure 3b indicates that the reorientation angle distribution for benzene molecules hopping among different adsorption sites is broad. This broad jump angle distribution and its effects on the associated benzene reorientation dynamics will be the object of further analysis below.

Orientational Autocorrelation Functions. While insights into the geometry of a slow molecular jump process(es) can be obtained directly from a single static 2D exchange spectrum, information on the time scales of such reorientation events requires that a series of spectra or stimulated echoes be acquired as a function of the mixing time. Correlation functions represent a simple and convenient means for characterizing stochastic processes, such as benzene hopping among adsorption sites inside the cavities of a nanoporous zeolite crystallite. One experimentally accessible class of orientational autocorrelation
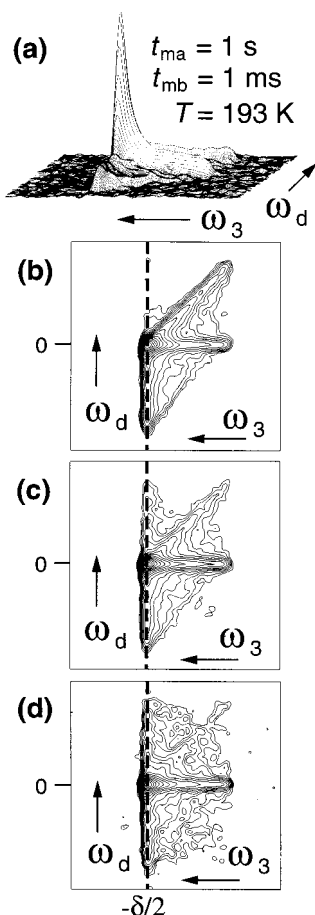
Benzene Adsorbed on Ag−Y Zeolite

J. Phys. Chem. A, Vol. 103, No. 34, 1999 **6695**

Figure 5. Experimental 3D DICO ^{13}C NMR spectra for benzene adsorbed on Ag−Y zeolite, acquired using the pulse sequence shown in Figure 2d. Stacked plot (a) and contour plot (b) of the spectrum acquired at $T = 193$ K and with $t_{ma} = 1$ s and $t_{mb} = 1$ ms. Significant molecular reorientation has occurred during t_{ma} but not t_{mb}, resulting in asymmetry with respect to the difference frequency $\omega_d = \omega_1 - \omega_2 = 0$. This asymmetry can be quantified by taking the ratio of spectral intensity $G(x)$ along the dashed line at $\omega_3 = -\delta/2$. As the second mixing time is increased to (c) $t_{mb} = 100$ ms and (d) $t_{mb} = 500$ ms, the spectra become more symmetric, reflecting a loss of correlation in molecular orientations before and after t_{mb}.

functions is given by $C_L(t_m)$:[7b,21]

$$C_L(t_m) = (2L + 1)\langle P_L(\cos(\beta(t=0)))P_L(\cos(\beta(t=t_m)))\rangle \quad (3)$$

where $L = 2, 4, \ldots$ denotes the order of the corresponding Legendre polynomial $P_L(\cos(\beta))$. For $L = 2$, the decay of $C_2(t_m)$ with increasing mixing time t_m is primarily sensitive to large-angle motions. In the special case of $\eta = 0$ (an axially symmetric interaction tensor), $C_2(t_m)$ is proportional to the two-time frequency average $\langle \omega_1 \omega_2 \rangle(t_m)$. For $\eta = 0$, the orientational autocorrelation function $C_2(t_m)$ can be obtained directly from 2D exchange ^{2}H or ^{13}C NMR spectra:

$$C_2(t_m) = \frac{5}{\delta^2}\langle \omega_1 \omega_2 \rangle(t_m) = \frac{5}{\delta^2}\int\int d\omega_1\, d\omega_2\, S(\omega_1,\omega_2;t_m)\omega_1\omega_2$$

$$(4)$$

The experimental spectral intensity $S(\omega_1,\omega_2;t_m)$ is integrated numerically, weighted by the product of the frequency coordinates of the individual points. Higher even-order correlation functions $C_L(t_m)$ may be obtained by expressing $P_L(\cos\beta)$ in terms of $P_2(\cos\beta) = \omega/\delta$.[21]

2D and 4D Echo Signals. The geometrical aspects of molecular reorientation, particularly small-angle motions, can
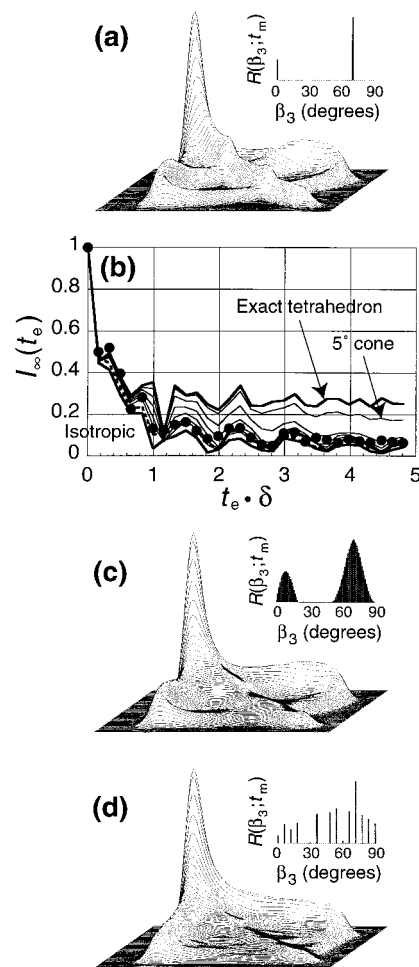

Figure 6. (a) Simulated 2D exchange spectrum calculated for a jump motion between four identical and exactly tetrahedrally arranged sites with $t_m \gg \tau_c$, i.e., conditions where full exchange prevails. The corresponding reorientation angle distribution $R(\beta_3;t_m)$ is shown as an inset. (b) The final-state structure factor $I_\infty(t_e)$ at $T = 298$ K is plotted together with simulated curves for exact tetrahedral jumps, jumps between the caps of cones with opening angles varying from 5° to 30° in 5° increments around the axis of a tetrahedron, an isotropic distribution, and the distribution resulting from a direct expansion of the experimental spectrum shown in Figure 3b (dashed line). Molecular exchange among tetrahedrally arranged cone caps with 20° opening angles appears to provide a reasonable fit to the data. (c) Simulated 2D exchange spectrum and reorientation angle distribution (inset) calculated for jumps between cone caps with 20° opening angles. This simulated spectrum resembles more closely the experimental 2D exchange ^{13}C NMR spectrum of Figure 3b than the simulation for an exact tetrahedral jump process displayed in Figure 6a. (d) Simulated 2D exchange spectrum calculated via a 6°-resolution direct expansion of the experimental spectrum shown in Figure 3b. The corresponding reorientation angle distribution $R(\beta_3;t_m)$ (weighting factors that yield the best fit) is shown as an inset. Intensity contributions from medium reorientation angles provide evidence for the participation of nontetrahedrally arranged adsorption sites in benzene reorientation dynamics. Gaussian damping of 800 Hz was applied to each of the simulated spectra, consistent with that used in processing the experimental spectra in Figure 3.

be probed in detail by exploiting the stimulated echoes present in 2D exchange time-domain data.[7b,9,21,29] In the pulse sequence of Figure 2b, a stimulated echo is formed at time $t_e \equiv t_2 = t_1$ after the start of the detection period. The intensity of the echo signal $s(t_1=t_2=t_e;t_m)$ is reduced due to T_1 and T_2 relaxation, with molecular reorientation during the mixing time causing additional echo signal decay.

The time scales of slow molecular reorientation motions can

be characterized by following the decay of the stimulated echo intensity with increasing mixing time for a particular value of t_e, after accounting for relaxation. Echo data for spectral patterns of different widths (different δ values), but with interaction tensors having identical axial symmetries (η), can be compared directly by using the quantity $t_e \cdot \delta$. The signals $\langle \cos(\omega_1 t_e) \cos(\omega_2 t_e) \rangle$ and $\langle \sin(\omega_1 t_e) \sin(\omega_2 t_e) \rangle$ are measured using the pulse sequence in Figure 2b by adjusting the phase of the $\pi/2$-pulse preceding the mixing time t_m in two separate experiments; combining the two signals yields $\langle \cos((\omega_1 - \omega_2)t_e) \rangle$. For sufficiently small values of t_e (≤ 50 μs for the present ^{13}C case with $\delta = -5.53$ kHz at 4.2 T), the $\langle \sin(\omega_1 t_e) \sin(\omega_2 t_e) \rangle$ signal is proportional to $\langle \omega_1 \omega_2 \rangle(t_m)$. In the case of an axially symmetric interaction tensor ($\eta = 0$), the $\langle \sin(\omega_1 t_e) \sin(\omega_2 t_e) \rangle$ signal acquired with a small value of t_e is also proportional to $C_2(t_m)$.[30] In general, the stimulated echo acts as a "filter"; by varying t_e, the experiment becomes sensitive to different reorientation geometries.[29] For small values of t_e, only large-angle reorientations lead to changes in the NMR frequencies that are sufficiently large to be detected. The echoes become more sensitive to small-angle motions at larger values of t_e. One method of probing large-angle motions is shown in Figure 4, which compares the echo signal intensity of $\langle \cos((\omega_1 - \omega_2)t_e) \rangle$ for $t_e = 150$ μs and the correlation function $C_2(t_m)$ for the case where the normals to the aromatic planes of all benzene molecules reorient by the angle β_3. The echo signal obtained when $t_e = 150$ μs is more sensitive to small-angle motions than $C_2(t_m)$, with the result that small-angle motions that are slightly faster than the large-angle motions will cause the echo intensity to decay more quickly than $C_2(t_m)$.

The existence of a distribution of molecular reorientation rates can be confirmed by a series of reduced 4D exchange NMR spectra[21,31] or 4D time-domain echo signals,[32] acquired using the pulse sequence in Figure 2c. The 4D time-domain echo signals are sensitive to molecular reorientation motions during t_{ma} and t_{mc}, but not during t_{mb}. However, during t_{mb} the process of rate exchange, i.e., slowly reorienting molecules becoming rapidly reorienting molecules and vice versa, will reduce the 4D echo intensity. Typically, the signals $\langle \cos(\omega_1 t_e) \cos(\omega_2 t_e) \cos(\omega_3 t_e) \cos(\omega_4 t_e) \rangle$ and $\langle \sin(\omega_1 t_e) \sin(\omega_2 t_e) \cos(\omega_3 t_e) \cos(\omega_4 t_e) \rangle$, with $t_e \equiv t_4 = t_3 = t_2 = t_1$, are combined and corrected for relaxation effects to yield $F_{4,\cos}(t_{ma}, t_{mb}, t_{mc}) = \langle \cos((\omega_1 - \omega_2)t_e) \cos(\omega_3 t_e) \cos(\omega_4 t_e) \rangle$, which is a reasonable approximation to $F_4(t_{ma}, t_{mb}, t_{mc}) = \langle \cos((\omega_1 - \omega_2)t_e) \cos((\omega_3 - \omega_4)t_e) \rangle$. Setting $t_{ma} = t_{mc}$ and dropping them from the list of arguments, $F_4(t_{mb})$ is constant as t_{mb} is increased, provided all molecules reorient with a single rate.[33] On the other hand, rate exchange causes $F_4(t_{mb})$ to decay. Such rate exchange can be quantified by invoking a rate memory parameter Q, which represents the average number of hops that a slow molecule executes before it "forgets" its initial dynamic state.[32] Writing the relaxation-corrected 2D signal $\langle \cos((\omega_1 - \omega_2)t_e) \rangle$ as $F_2(t_m)$, Q can be quantified by fitting the data to the approximate analytical expression[32]

$$F_4(t_{mb}) = F_2\left(t_{ma} + \frac{t_{mb}}{Q} + t_{mc}\right) + \frac{\left[F_2(t_{ma}) - F_2\left(t_{ma} + \frac{t_{mb}}{Q}\right)\right]\left[F_2(t_{mc}) - F_2\left(t_{mc} + \frac{t_{mb}}{Q}\right)\right]}{1 - F_2\left(\frac{t_{mb}}{Q}\right)}$$ (5)

As an alternative to eq 5, the dependence of $F_4(t_{mb})$ on Q can be calculated more precisely by using the numerical method described in ref 32a.

Three-Dimensional Difference Correlated Exchange Spectroscopy. Despite their high information contents, series of 2D exchange spectra may nevertheless still not have sufficient resolution and sensitivity to yield an unambiguous kinetic description of the motions leading to a broad distribution of reorientation angles. As an example, 2D exchange ^{2}H NMR spectra of polystyrene above the glass transition can be fit equally well with two different models, one involving rotational diffusion with a log-normal distribution of correlation times, and the other including large-angle jumps.[34] To aid in separating multiple reorientation processes, the three-dimensional (3D) difference correlated exchange spectroscopy (DICO) NMR experiment can be used, with accompanying measurement time requirements that are only slightly longer than for 2D exchange spectra.[25] In particular, the DICO experiment (Figure 2d) can establish whether the orientations of molecules during the detection period t_3 are correlated with their orientations during an intermediate evolution time t_2 with respect to the dynamics possible during t_{ma}.[25b] This is achieved by acquiring 2D spectra that correlate frequency changes during t_{ma} (as monitored by difference frequencies $\omega_d = \omega_1 - \omega_2$) with frequencies ω_3 (corresponding to molecular orientations) in the detection period. In a powder sample, large-angle reorientations during t_{ma} result in spectral intensity at both large and small values of ω_d, whereas small-angle reorientations yield spectral intensity only at small values of ω_d.

It is possible to model stimulated echo data to quantify the relative rates of small- and large- angle jumps for benzene adsorbed on a zeolite, as shown by Isfort et al.,[9] though this requires the use of a model in conjunction with data measured as functions of the mixing time t_m and echo time t_e. The DICO experiment, however, establishes whether the rates of small-angle reorientation motions are faster, slower, or the same as those associated with large-angle reorientation. Moreover, the analysis does not require a model of the motion. When significant molecular reorientation occurs predominantly during the first mixing time t_{ma} of a DICO experiment, the spectrum (Figure 5a–c) will be highly asymmetric in the $\omega_d = \omega_1 - \omega_2$ dimension. When molecular orientations before and after t_{mb} are uncorrelated, the DICO spectrum will be symmetric with respect to the slice $\omega_d = 0$. The degree of symmetry can be characterized by $G(x)$, the ratio of the spectral intensities on opposite sites of the spectrum with respect to $\omega_d = 0$, where $x = \omega_d/\delta$. In most cases, the $\omega_3 = -\delta/2$ slice indicated by the dotted lines in the contour plots of Figure 5b–d is suitable for analysis. If small-angle motions are faster than large-angle motions, the ratio of intensities $G(x)$ will be larger at small values of x. If large-angle motions are faster than small-angle motions, then $G(x)$ will be higher at large values of x, while $G(x)$ will be flat when small- and large-angle reorientations occur with equal rates.

Intermediate Dynamic Regime. Molecular reorientations with time scales shorter than about 10^{-3} s can be characterized by modeling the distortion and averaging effects of these motions on NMR spectra of powder samples. In the fast regime, where reorientation is rapid compared to the reciprocal coupling strength of the nuclear interaction ($1/\delta$), i.e., reorientation rates are much faster than the width of the NMR line shape, motion results in an averaged interaction tensor that depends on the geometry of reorientation. For example, motionally averaged ^{1}H, ^{2}H, and ^{13}C NMR line shapes[7,35,36] observed for benzene adsorbed on X-type zeolites are consistent with rapid rotation of benzene molecules about their 6-fold axes perpendicular to their aromatic planes. Such rotational motion is similarly

Benzene Adsorbed on Ag−Y Zeolite

J. Phys. Chem. A, Vol. 103, No. 34, 1999 **6697**

observed for benzene adsorbed on Ag−Y zeolite, which yields an averaged axially symmetric ($\eta = 0$) ^{13}C chemical shift tensor.

However, in the intermediate dynamic regime, where reorientation time scales are on the order of $1/\delta$, the assumption that NMR frequencies are constant during an echo pulse sequence (Figure 2e) or subsequent detection period may no longer be valid. In this case, molecular reorientation must be considered explicitly during the various time periods of an NMR experiment. This can be done by modeling the reorientation as a stationary Markov process[21] characterized by an exchange matrix $\mathbf{\Pi}$, whose off-diagonal elements Π_{lm} represent exchange probabilities (jump rates) from site m to site l. Solving an appropriate system of kinetic equations typically results in expressions for NMR time-domain signals with matrices in exponential terms, which are normally evaluated numerically via matrix diagonalization. The expressions given below neglect relaxation effects, i.e., multiplication by $\exp(-t/T_2)$, which can be easily included if necessary. Model calculations are evaluated by comparing the fits of simulations to the experimental spectra. In general, NMR line shapes alone do not provide sufficient information to uniquely determine complicated motions that involve distributions of molecular reorientation time scales and geometries. However, 2D exchange ^{13}C NMR time-domain data and spectra obtained at lower temperatures can be used to constrain models for molecular reorientation occurring over intermediate dynamic time scales.

Static Solid-Echo ^{2}H NMR Spectra. For solid-echo ^{2}H NMR spectra of systems with motional processes occurring in the intermediate dynamic regime, the times before and after the echo pulse, t_{pre} and t_{post}, respectively, are considered explicitly by writing the contributions to the time-domain signal as[18,21,27]

$$g(t_{\text{pre}},t_{\text{post}}) = \mathrm{e}^{(\mathbf{\Pi}-\mathrm{i}\boldsymbol{\omega})t_{\text{post}}}\, \mathrm{e}^{(\mathbf{\Pi}+\mathrm{i}\boldsymbol{\omega})t_{\text{pre}}} P_1 \qquad (6)$$

where $\boldsymbol{\omega}$ is a diagonal matrix of NMR frequencies at different sites expressed in a common reference frame as a function of the Euler angles (α,β,γ), and P_1 represents the equilibrium site-occupation probabilities. The total signal is obtained by integrating over all orientations using the Euler angles (α,β,γ) and then summing the contributions to $g(t_{\text{pre}}, t_{\text{post}})$ from the different sites.

Magic-Angle Spinning ^{13}C NMR Spectra. In the intermediate dynamic regime, ^{13}C MAS spectra are affected by frequency changes due to both sample spinning and molecular reorientation. The appropriate system of kinetic equations can be solved numerically.[37] Another approach is to calculate contributions to the time-domain signal using a Fourier-like series expansion in periodic frequency terms $\mathrm{e}^{\mathrm{i}N\omega_{\mathrm{R}}t}$:[38]

$$g(t) = \sum_{l,m} \sum_{N=-\infty}^{\infty} [\mathrm{e}^{-\mathrm{i}\mathbf{H}_{\mathrm{F}}t}]_{lN,m0}\, \mathrm{e}^{\mathrm{i}N\omega_{\mathrm{R}}t} P_m \qquad (7)$$

Integration over the Euler angles (α,β,γ), followed by summation of the contributions from different sites, yields the total time-domain signal. The Floquet Hamiltonian $\mathbf{H}_{\mathrm{F}}$ is a super-matrix composed of Z^2 submatrices, where molecules reorient among Z discrete sites. The Z submatrices along the diagonal of $\mathbf{H}_{\mathrm{F}}$ contain both isotropic and anisotropic contributions to the NMR frequencies at each site, as well as $N\omega_{\mathrm{R}}$ terms and the diagonal elements of the exchange matrix. The off-diagonal submatrices of $\mathbf{H}_{\mathrm{F}}$ express the off-diagonal elements of the exchange matrix. Each submatrix of $\mathbf{H}_{\mathrm{F}}$ has dimensions N by N, with N varying from $-\infty$ to ∞. In practice, each submatrix is truncated; dimensions 13 by 13, corresponding to $N = -6$ to $+6$, were used for each submatrix in this study.

Results and Discussion

Geometry of Benzene Site-Hopping in Ag−Y. The geometry that underlies the site-hopping motions of benzene adsorbed on Ag−Y zeolite is revealed by modeling 2D exchange spectra and stimulated echo data in Figures 3 and 6, respectively. A broad distribution of molecular reorientation angles is directly observable in the experimental data, which can be probed in more quantitative detail using model analyses. For example, Figure 6a shows a simulated 2D exchange spectrum calculated for a jump motion among four equivalent, tetrahedrally arranged sites in the full exchange limit ($t_{\mathrm{m}} \rightarrow \infty$). The reorientation angle distribution $R(\beta_3;t_{\mathrm{m}})$ is shown as an inset. For $\eta = 0$, this distribution uniquely determines the 2D spectrum according to[21,39]

$$S(\omega_1,\omega_2;t_m) = \int_{0°}^{90°} \mathrm{d}\beta_3\, R(\beta_3;t_m)\, S_{\beta_3}(\omega_1,\omega_2) \qquad (8)$$

This integral represents the sum of the subspectra for each reorientation angle, $S_{\beta_3}(\omega_1,\omega_2)$, weighted by factors $R_{\mathrm{f}}(\beta_3;t_{\mathrm{m}})$ for $0° \leq \beta_3 \leq 180°$. Due to the equivalence of the spectra for β_3 and $180° - \beta_3$, integration is restricted to $0° \leq \beta_3 \leq 90°$:

$$R(\beta_3;t_m) = R_{\mathrm{f}}(\beta_3;t_m) + R_{\mathrm{f}}(180° - \beta_3;t_m) \qquad (9)$$

For a narrow reorientation angle distribution, the simulation contains a clear elliptical off-diagonal ridge that is not observed in the experimental spectrum of Figure 3b. The absence of a well-defined elliptical pattern in Figure 3b directly reflects a broad distribution of benzene jump reorientation angles among adsorption sites in Ag−Y zeolite.

The normalized NMR time-domain stimulated echo intensity in the limit of $t_{\mathrm{m}} \rightarrow \infty$, corrected for relaxation effects, is called the final-state structure factor, $I_\infty(t_{\mathrm{e}})$.[29] It provides more detailed insight on the broad reorientation angle distribution observed for benzene site-hopping in Ag−Y. Figure 6b shows $I_\infty(t_{\mathrm{e}})$ obtained from 2D exchange ^{13}C time-domain data measured off-resonance at $T = 193$ K. Accompanying the experimental results (filled circles) are simulations for several candidate models, including exact tetrahedral jumps, jumps among tetrahedrally arranged cone caps with different cone opening angles, a jump distribution from a direct expansion of the spectrum in Figure 3b (see below), and a completely isotropic distribution. For large values of t_{e}, the curve simulated for jumps between exact tetrahedral positions approaches the limit 0.25. The experimentally observed values fall well below this value and follow the curves that were calculated for random jumps between cone caps, whose opening angles are estimated to be not less than 15°. However, values for larger cone-opening angles overlap. While the final-state structure factor $I_\infty(t_{\mathrm{e}})$ provides excellent discrimination among various small deviations from exact tetrahedral jumps, it is less sensitive to differences in models with very broad distributions, i.e., cone-opening angles greater than 20°. However, an isotropic distribution, with $R_{\mathrm{f}}(\beta_3;t_{\mathrm{m}}\rightarrow\infty) = \sin(\beta_3)$, yields values of $I_\infty(t_{\mathrm{e}})$ in Figure 6b that consistently fall below the experimental points. The presence of the ridge-like feature running along the diagonal in the experimental spectrum in Figure 3b provides further evidence that an isotropic distribution can be rejected. If the reorientation geometry were isotropic, the diagonal ridge would disappear as $t_{\mathrm{m}} \rightarrow \infty$.[21]

To differentiate among the various models that invoke large cone-opening angles, the experimental exchange ^{13}C NMR spectrum in Figure 3b was compared with simulated spectra. The closest fit, calculated with a cone-opening angle of 20°, is shown in Figure 6c. Increasing the cone-opening angle causes

the diagonal to broaden and eventually disappear, while smaller cone-opening angles yield values of $I_\infty(t_e)$ that are too large compared to the experimental values indicated in Figure 6b. From the combined analyses of time-domain echoes and simulations of an experimental 2D exchange spectrum, a cone-opening angle between 15° and 25° provides a reasonable description of the disorder associated with the distribution of benzene jump angles. A cone-opening angle of 20° lies between values obtained for two related benzene/zeolite systems. The benzene/Ag−Y reorientation angle distribution is about twice as wide as observed for benzene adsorbed on Ca−LSX zeolite (Si/Al = 1.0) at the same loading (2 molecule/supercage, ref 7b) and about a factor of 1.3 more narrow than measured for benzene on Na−Y zeolite (Si/Al = 2.85) near saturation coverage.[9] However, small discrepancies between the experimental and simulated spectra are still noticeable for the cone-cap model. For example, the diagonal of the simulated spectrum in Figure 6c is not as well-defined and the off-diagonal patterns in the simulation are sharper compared to those features in the experimental spectrum (Figure 3b).

An alternative approach to characterizing the reorientation angle distribution is a direct expansion of the experimental 2D exchange spectrum using a series of simulated subspectra $S_{\beta_3}(\omega_1,\omega_2)$ for different discrete reorientation angles β_3. This expansion is essentially a discrete version of eq 8 (refs 21 and 40) and results in a series of weighting factors $R(\beta_3;t_m)$, that are constrained to be nonnegative. A direct expansion of the spectrum in Figure 3b using 16 subspectra (0−90° in 6° steps) is shown in Figure 6d. The largest weighting factor is for $\beta_3 = 72°$, consistent with the tetrahedral and inverse tetrahedral arrangement of SII and window sites. However, intensity contributions at medium reorientation angles, namely $\beta_3 = 36°$, 48°, and 54°, suggest the participation of additional adsorption sites in benzene site-hopping processes. If Ag$^+$ cations are located at other sites within the Ag−Y supercages, these sites are likely to be at positions of lower-symmetry than the SII sites and would be expected to give rise to a number of new benzene reorientation angles. This is supported by simulations of related systems, which reveal numerous discrete reorientation geometries. For example, in the case of benzene adsorbed on Na−X zeolite, molecular docking calculations[41] yield additional jump angles of 20°, 90°, 111°, and 124° for reorientation of benzene molecules from SIII cations to one of four possible SII adsorption sites within the same supercage. Furthermore, the SIII cation perturbs the orientation of benzene adsorbed at the nearby window site, yielding reorientation angles of 11°, 103°, 105°, and 120° for jump motions between a window and nearby SII sites (as well as 120° for reorientation from a window to an SIII site). Likewise, Ag$^+$ cations located at sites other than SII sites, yet still accessible to benzene adsorbed on Ag−Y zeolite, would introduce other reorientation angles. Furthermore, such Ag$^+$ cations, and perhaps even hydroxyl defects in the Ag−Y zeolite framework, could cause an adjustment in the angle at which a benzene molecule adsorbs at a nearby site. Unfortunately, the experimental spectrum of Figure 3b has insufficient resolution to pinpoint the location of additional adsorption sites that likely participate in benzene reorientation dynamic processes.

Modeling the broad reorientation angle distribution, in the limit of a long mixing time, as tetrahedrally arranged cone caps also does not uniquely specify the kinetic processes leading to this distribution. There are several possibilities that could lead to benzene reorientation geometries on Ag−Y zeolite that are consistent with the long mixing time experimental 2D exchange
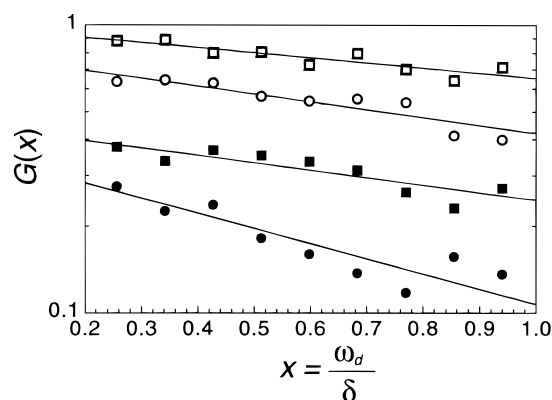

Figure 7. Semilog plot of intensity ratios $G(x)$ obtained from 3D DICO ^{13}C NMR spectra of benzene/Ag−Y with a fixed first mixing time $t_{ma} = 1$ s, and different values for the second mixing time t_{mb} of 1 ms (filled circles), 10 ms (filled squares), 100 ms (open circles), and 500 ms (open squares). Each data point represents an average of spectral intensity from a 3 × 3 grid of nine points on one side of the spectrum ($\omega_d > 0$) ratioed to the average of nine points on the opposite side of the spectrum ($\omega_d < 0$). Fits of straight lines are intended as guides to the eye, showing negative slopes, which establish that small-angle reorientation motions are somewhat faster than large-angle reorientations. Data for $x < 0.2$ are not shown due to interference from spectral broadening of the $\omega_d = \omega_1 - \omega_2 = 0$ feature, which reflects ^{13}C NMR frequencies that were the same before and after the first mixing time t_{ma}. Data for $x > 1.0$ corresponding to very large angle reorientations are not included because of low signal intensity in the spectra far away from $\omega_d = 0$.

^{13}C spectrum and stimulated echo data shown in Figures 3b and 6b. One possibility is that molecules hopping among tetrahedrally arranged adsorption sites execute only large-angle jumps that are not exactly 109.5°, such that upon return to the original adsorption site (or another orientationally equivalent site), the net reorientation angle is offset from 0°. A second possibility is that, due to attractive interactions among neighboring benzene molecules, small-angle adjustments occur when a neighboring benzene molecule executes a large-angle hop between two adsorption sites.[42] A third possibility is that small-angle motions, such as those calculated in ref 43, arise from a process that is independent of large-angle jumps. Finally, as indicated by the simulated spectrum obtained via direct expansion (Figure 6d), the overall arrangement of adsorption sites may not be precisely tetrahedral. In the related benzene/Ca−LSX system, where the arrangement of the benzene adsorption sites is tetrahedral,[7b,44] the reorientation angle distribution is significantly narrower.

Additional insight into these benzene reorientation motions (changes in the orientations of the aromatic ring normals) is provided by examination of the stimulated echoes as a function of mixing time. If the rates of small-angle aromatic plane motions are much slower than those for large-angle site-hopping processes, correlation times at large and small values of t_e will be nearly identical. However, in the case of benzene reorientation on Ag−Y zeolite, correlation times at large values of t_e are shorter than at small values of t_e (data not shown), implying that small-angle motion rates are comparable or larger in magnitude than large-angle reorientation rates.

Further support for this observation is provided by a series of four DICO ^{13}C spectra, acquired at $T = 193$ K with second mixing times of $t_{mb} = 1$, 10, 100, or 500 ms. Figure 7 shows a plot of the intensity ratios $G(x)$ of the DICO spectra as a function of $x = \omega_d/\delta$. The relative spectral intensities about $\omega_d = \omega_1 - \omega_2 = 0$ (the ratio $0 \leq G(x) \leq 1$) provide information about orientational correlations and their dependence on the reorienta-
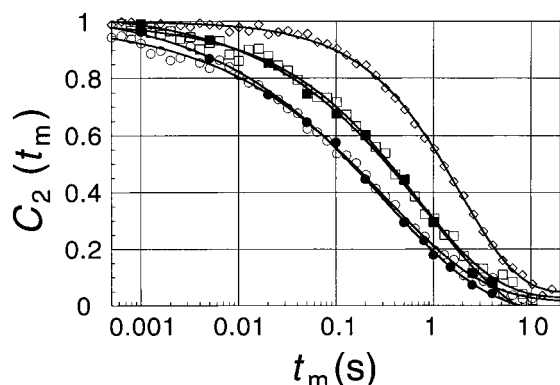
Benzene Adsorbed on Ag−Y Zeolite

J. Phys. Chem. A, Vol. 103, No. 34, 1999 **6699**

Figure 8. Semilog plot of the correlation function $C_2(t_m)$ versus mixing time t_m for benzene/Ag−Y. Data acquired at 193 K (circles) and 183 K (squares) were obtained both from static 2D exchange ^{13}C NMR spectra (filled symbols) and ^{13}C stimulated echoes with $t_e = 50$ μs (open symbols), showing excellent agreement between the two methods. The shape of the decay of $C_2(t_m)$ measured at 153 K using stimulated echoes (open diamonds) more closely resembles a single exponential than the higher-temperature data. This change in shape at low temperature is consistent with the onset of spin diffusion, indicating that at 183 and 193 K molecular reorientation is the dominant process contributing to ^{13}C NMR frequency changes.

tion angles β_3, or analogously, the dependence of orientational correlations on ω_d or the dimensionless quantity $x = \omega_d/\delta$. The intensity ratios $G(x)$ for parts of the spectra at large values of the difference frequency ω_d (large values of x) are generally smaller than the ratios $G(x)$ near $\omega_d = 0$, proving that small-angle motions of the aromatic ring normals are faster than large-angle jump reorientations (see above). These results are consistent with separate analyses and model calculations of ^{2}H stimulated echoes for benzene adsorbed on Na−Y zeolite, which showed that the rates of the small-angle motions were approximately 2 times faster than the rates of the large-angle jump motions.[9] Furthermore, the ratio of small- and large-angle reorientation rates was independent of temperature, suggesting that the observable small-angle motions are not due to an independent stochastic process(es).[9] These results collectively indicate that small-angle adjustments as neighboring benzene molecules hop likely provide a significant contribution to the small-angle motions of benzene adsorbed on Ag−Y zeolite.

Time Scales of Benzene Site-Hopping. To investigate the temperature dependence of site-hopping dynamics for benzene adsorbed on Ag−Y zeolite, static 2D exchange ^{13}C, MAS ^{13}C, and static quadrupolar echo ^{2}H NMR experiments were performed on Ag−Y samples containing on average two benzene molecules per Ag−Y supercage. Static 2D exchange ^{13}C NMR spectra were analyzed using the orientational autocorrelation function $C_2(t_m)$, and the resulting nonexponential decay indicates a distribution of molecular reorientation rates, as confirmed by reduced 4D echo NMR experiments (see below).

Benzene jump reorientations among Ag$^+$ SII or window adsorption sites result in large-angle motions, while small-angle reorientation motions (not necessarily involving site-hopping) also occur. As shown in Figure 4 and as previously discussed, the correlation function $C_2(t_m)$ is sensitive to large-angle motions and less sensitive to small-angle motions, so that $C_2(t_m)$ can be used to analyze large-angle benzene site-hopping dynamics. For example, Figure 8 shows the decay of the correlation function $C_2(t_m)$, obtained from both 2D exchange ^{13}C NMR spectra and stimulated echo data. While the values of $C_2(t_m)$ obtained from 2D exchange spectra and stimulated echo data are consistent, the reduced measurement time requirements of the stimulated echo technique permit many more points to be obtained. If the

^{13}C NMR frequency changes during the mixing time are due to a single process, such as molecular reorientation among equivalent and equally populated sites, $C_2(t_m)$ decays mono-exponentially to a plateau value that contains information about the reorientation angle(s) and the number of participating sites.[21,45] More complicated behavior results if several inequivalent processes contribute to the NMR frequency changes, as is the case for the nonmonoexponential behavior of $C_2(t_m)$ shown in Figure 8. In the related benzene/Ca−Y (Si/Al = 2.0) system, two site-hopping processes (intra- and intercage motions) have been separated and individually quantified.[4] However, the number of motional processes occurring for benzene adsorbed on Ag−Y zeolite does not permit the individual molecular motions to be disentangled. Nevertheless, the $C_2(t_m)$ data can be fit with a general function, such as a stretched exponential (Figure 8):[46,47]

$$C_2(t_m) = (1 - C_2^\infty)e^{-(t_m/\tau_0)^\phi} + C_2^\infty \tag{10}$$

which provides general information on the overall geometries and time scales of the motions. The observed plateau values, $C_2^\infty \sim 0$, are consistent with a site-hopping geometry corresponding to reorientation among tetrahedrally arranged cone caps.

Although the experimental data points $C_2(t_m)$ are insufficient to distinguish among and separately quantify the different rates of ^{13}C NMR frequency changes, the fit parameter ϕ indicates the width of the rate distribution, once the general form of the distribution has been assumed. The form of the rate distribution may be calculated using ref 47 or 48 or, because the rate distribution is broad, it may be assumed to be Gaussian in the logarithm of the reorientation rate.[49] The values of τ_0 and ϕ from the fits are compiled in Table 1. The values of ϕ for $T \geq 163$ K are in the range 0.4−0.6 ($0 \leq \phi \leq 1$); for the mixing times used, these data are consistent with a log-normal distribution with a full-width-half-maximum (fwhm) of about 1.9 decades. The higher value of $\phi = 0.73 \pm 0.02$ obtained at 153 K is consistent with the onset of spin diffusion, which is expected to contribute a temperature-independent mono-exponential ($\phi = 1$) decay in $C_2(t_m)$.[7b,21] The variation of $C_2(t_m)$ with temperature indicates that at higher temperatures, such as 183 K and above, the dominant process affecting $C_2(t_m)$ is thermally activated molecular reorientation.

The nonexponential behavior ($\phi \neq 1$) of $C_2(t_m)$ reflects a distribution of benzene molecular reorientation rates on Ag−Y zeolite. Proof of a rate distribution is established in Figure 9, which presents results from a reduced 4D ^{13}C NMR experiment that measures the rate memory associated with the site-hopping motions of benzene molecules. Specifically, Figure 9 shows the decay of the normalized intensity, $F_{4,cos}(t_{mb})$, of the reduced 4D ^{13}C NMR echo signal corrected for relaxation effects, as a function of the duration of a second mixing time t_{mb} (Figure 2c). The decay of $F_{4,cos}(t_{mb})$ below a value of unity not only proves the existence of a rate distribution, but also provides evidence for rate exchange within the distribution as well; i.e., slowly reorienting molecules becoming rapidly reorienting molecules and vice versa. The rate memory parameter Q, the average number of jumps a "slow" molecule executes before its reorientation rate becomes uncorrelated with its initial slow rate, is quantified by using the decay of the 2D echo signal $F_2(t_m)$, also shown in Figure 9. For benzene adsorbed on Ag−Y zeolite, the decay of $F_{4,cos}(t_{mb})$ is consistent with $Q = 1$ calculated using eq 5.[50] This indicates that slowly reorienting benzene molecules experience changes in site-hopping reori-

TABLE 1: Results of Fitting Eq 10 to the Correlation Function $C_2(t_m)$ Obtained from $\langle\sin(\omega_1 t_e)\sin(\omega_2 t_e)\rangle$ ^{13}C NMR Stimulated Echo Data and 2D Exchange ^{13}C NMR Spectra (Eq 4)[a]

T (K)	^{13}C NMR stimulated echoes			2D exchange ^{13}C NMR spectra		
	τ_0 (s)	ϕ	C_2^∞	τ_0 (s)	ϕ	C_2^∞
153	1.92 ± 0.05	0.73 ± 0.02	0.04 ± 0.02			
163	1.72 ± 0.12	0.57 ± 0.02	0.01 ± 0.02	1.94 ± 1.40	0.47 ± 0.10	-0.08 ± 0.20
173	1.09 ± 0.05	0.58 ± 0.02	0.04 ± 0.02			
183	0.67 ± 0.04	0.53 ± 0.02	0.02 ± 0.02	0.86 ± 0.28	0.45 ± 0.05	-0.08 ± 0.09
193	0.33 ± 0.02	0.43 ± 0.02	0.01 ± 0.02	0.32 ± 0.03	0.41 ± 0.03	-0.03 ± 0.03

[a] The reduced measurement time requirements of the stimulated echo experiment permit acquisition of more data points, which results in significantly reduced measurement uncertainties compared to data obtained from the 2D exchange spectra.
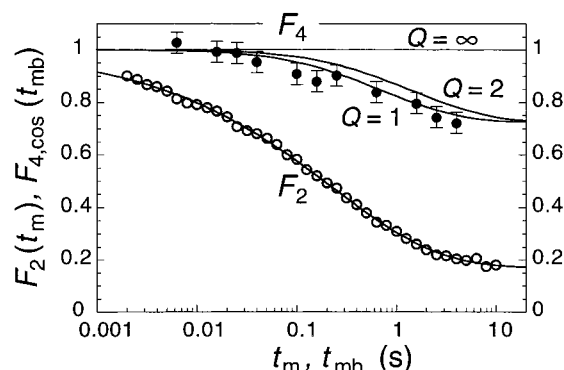
Figure 9. Plots of two-dimensional ($F_2(t_m)$, open circles) and four-dimensional ($F_{4,cos}(t_{mb})$, filled circles) stimulated echo ^{13}C NMR signal intensities acquired for benzene/Ag−Y at 193 K and with $t_e = 150$ μs, corrected for ^{13}C T_1 relaxation. A stretched exponential fit (see eq 10) to $F_2(t_m)$ yields $\tau_0 = 0.23 \pm 0.01$ s, $\phi = 0.40 \pm 0.02$, and a plateau value of 0.17 ± 0.01. The decay of $F_{4,cos}(t_{mb})$ below unity establishes the existence of a distribution of molecular reorientation rates and rate exchange between slowly and rapidly reorienting molecules. Application of eq 5 to $F_{4,cos}(t_{mb})$ yields a value of the rate memory parameter, $Q = 1$. This indicates that slowly reorienting molecules adopt, after on average one reorientation event, a new reorientation rate that is uncorrelated with their initially slow rate. Curves calculated for $Q = 2$ and $Q = \infty$ are shown for comparison.

entation rates typically after undergoing a single molecular jump. The overall rate distribution probably arises because of the existence of inequivalent benzene adsorption sites on Ag−Y zeolite, combined with benzene−benzene interactions and different local configurations (e.g., different numbers of benzene molecules in different supercages). Inequivalent benzene adsorption sites, such as Ag$^+$ SII cation and window sites, are located near each other and are dispersed throughout the Ag−Y crystallites. As a consequence, benzene exchange among such inequivalent sites is anticipated to occur frequently. While certain arrangements of adsorption sites or site blockage by other adsorbed benzene molecules might lead to $Q > 1$,[42,51] for most cases the minimum rate memory is reasonable and expected.

While slow benzene/Ag−Y molecular reorientation rates ($<10^3$ s^{-1}) were measured using exchange NMR techniques, more rapid rates of 10^3−10^5 s^{-1} can be quantified by modeling the distortion and averaging effects of these motions on MAS ^{13}C NMR spectra. As shown in Figure 10, the ^{13}C MAS spectrum acquired at 208 K shows a centerband peak with a fwhm of 100 Hz, located at the position of the isotropic chemical shift (126 ± 0.5 ppm), and a manifold of spinning sidebands at integer multiples of the spinning frequency, $\omega_R = 2\pi \times 1500$ Hz. Spectra acquired at temperatures of 185 and 197 K are identical to the MAS spectrum acquired at 208 K, which indicates that molecular site-hopping rates are slower than 10^3 s^{-1} at these temperatures. As the temperature is increased to 286 K, molecular reorientation broadens the ^{13}C MAS peaks. The presence of sharp peaks overlaying broader features in the
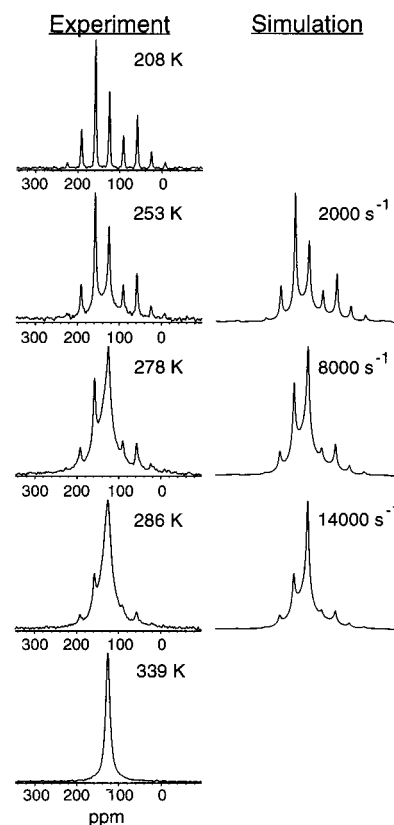

Figure 10. Variable-temperature experimental and simulated MAS ^{13}C NMR spectra for a bulk loading of two adsorbed benzene molecules per Ag−Y zeolite supercage. The numerical values accompanying the simulated MAS ^{13}C NMR spectra are the centers of a 1.9 decade fwhm log-normal rate distribution, which was varied to obtain the simulations.

spectra acquired at temperatures of 253−286 K is characteristic of the distribution of reorientation rates discussed above. At higher temperatures (>339 K), the chemical shift anisotropy is averaged away by rapid molecular reorientation. The fwhm of the centerband peak in the spectrum acquired at 339 K is 550 Hz (reduced to 300 Hz at 366 K), reflecting nearly complete averaging of the ^{13}C chemical shift anisotropy under these conditions.

As shown in Figure 10, simulated MAS spectra have been fit to the experimental MAS ^{13}C spectra acquired at the intermediate temperatures of 253, 278, and 286 K, as well as at 266, 298, and 312 K (not shown). The simulations used a model with twelve discrete sites arranged in three tetrahedra, rotated by 0°, 10°, and 20°, respectively, to approximate the overall reorientation geometry measured using 2D exchange ^{13}C NMR (Figures 3 and 6). To fit the experimental MAS spectra, simulations were calculated using a single reorientation rate[52] and then combined to yield log-normal rate distributions 1.9 decades fwhm. The center of this rate distribution on a
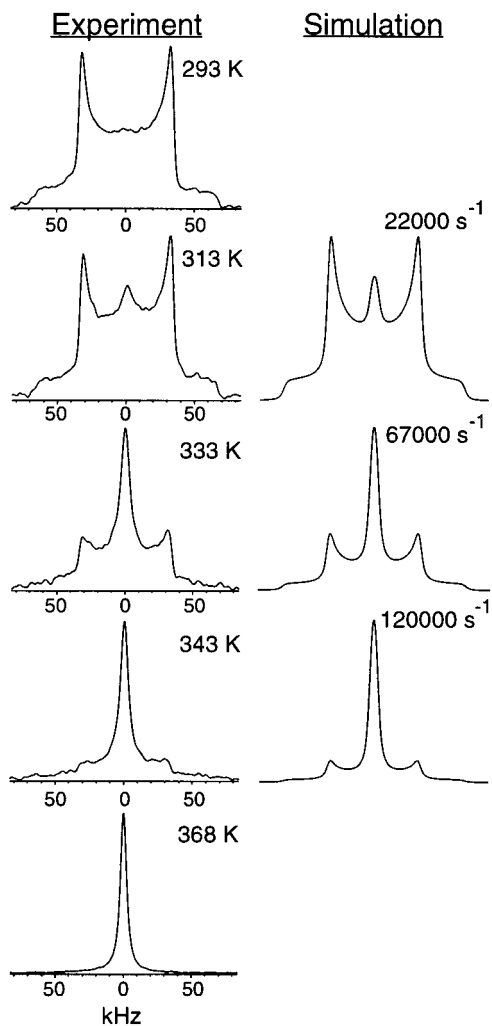
Figure 11. Variable-temperature experimental and simulated static ^{2}H NMR spectra for a bulk loading of two adsorbed benzene molecules per Ag−Y zeolite supercage. The numerical values accompanying the simulated static ^{2}H NMR spectra are the centers of a 1.9 decade fwhm log-normal rate distribution, which was varied to obtain the simulations.

Figure 12. Temperature dependence of the centers of the rate distributions for reorientation motions undergone by benzene adsorbed on Ag−Y zeolite. The summarized results were obtained by applying a log-normal rate distribution model to ^{2}H NMR line shapes (open triangles), ^{13}C MAS line shapes (filled diamonds), C_2 correlation functions obtained from ^{13}C stimulated echoes (filled circles), and 2D exchange ^{13}C NMR spectra (open squares). Experimental uncertainties in the centers of the rate distributions are about the size of the data points. The solid line in the diagram represents a fit of $\ln(k_0 e^{-E_a/RT} + k_{SD})$ to the combined data, corresponding to $E_a = 34$ kJ/mol, $k_0 = 2 \times 10^{10}$ s^{-1}, and $k_{SD} = 1.3$ s^{-1}, which parametrizes the net effects of all large-angle site-hopping motions on the reorientation rate distribution.

logarithmic scale was varied to adjust each fit, with the value used accompanying each respective simulated spectrum. The resulting simulated MAS ^{13}C NMR spectra in Figure 10 agree well with the experimental spectra. The slight discrepancies in line widths likely arise because the model does not precisely represent the complex experimental reorientation geometry and rate distributions. While other rate distributions are also consistent with the 2D exchange ^{13}C NMR and stimulated echo data, such as a distribution that is highly asymmetric on a logarithmic scale, they typically lead to apparent activation energies for benzene reorientation (see below) that differ by only a few kJ/mol.[53]

The absence of sidebands in the high-temperature ^{13}C MAS spectra indicates that the benzene reorientation geometry is highly symmetric. Reducing the symmetry of the model by removing one of the 12 sites results in the presence of residual sideband peaks even for very rapid ($\gg\delta$) reorientation rates, in contrast to the experimental spectra acquired at high temperature. The good fit between simulation and experiment at intermediate temperatures (253−286 K) shows that the 12-site geometry and 1.9-decade-wide rate distribution are a good model approximation of complicated benzene site-hopping dynamics on Ag−Y zeolite.
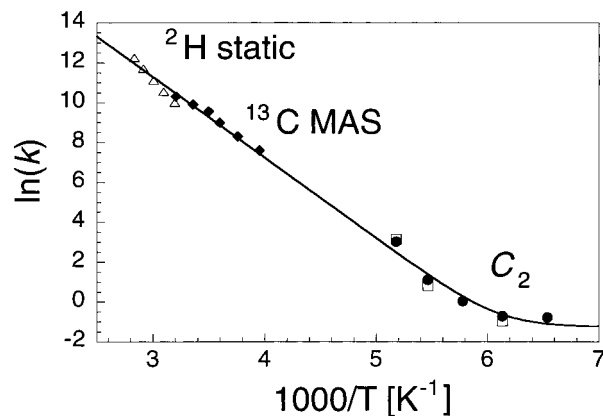
A further test of the 12-site model and rate distribution at higher temperatures is provided by fitting static ^{2}H NMR spectra. Because ^{2}H NMR spectra of benzene adsorbed on Ag−Y zeolite cover a significantly broader frequency range than their ^{13}C counterparts, static ^{2}H NMR spectra are sensitive to more rapid reorientation rates, 10^4 to 10^6 s^{-1}. Figure 11 compares simulations to experimental ^{2}H spectra, acquired over the temperature range 293−368 K with a 50 μs echo delay between the two $\pi/2$-pulses in Figure 2e. The ^{2}H simulations were obtained using the same model geometries and rate distributions as used for the ^{13}C MAS simulations (Figure 10) and included the effect of the 50 μs echo delay. The ^{2}H simulations agree well with the ^{2}H NMR data. As for the ^{13}C analyses, the model used is a reasonable approximation, though there are small discrepancies. The width of the central peak as well as in the intensities of "valleys" between the central peak and the "horns" of the ^{2}H powder patterns differ slightly between experimental and simulated spectra. The widths of the anisotropic line shapes determine the reorientation time scales of molecular reorientation that can be probed. The magnitude of the ^{13}C NMR interaction coupling strength is small ($\delta \sim 5.5$ kHz), while the ^{2}H NMR spectrum is broader ($\delta \sim 66$ kHz). Thus, the ^{13}C NMR spectrum is averaged to a single line at 339 K, while the ^{2}H NMR spectrum acquired at 343 K is distorted, but not yet completely averaged to a single line. Similar line shape analyses for probe species with anisotropic interaction strengths on the order of a few MHz (e.g., muon spin resonance[19]) are useful for even faster reorientation rates.

In combination, the collective and mutually consistent analyses of the static 2D exchange ^{13}C, MAS ^{13}C, and static ^{2}H NMR results allow the apparent site-hopping kinetics of benzene molecules adsorbed on Ag−Y zeolite to be established. Fitting the log-normal rate distribution model to these data yields the Arrhenius plot in Figure 12. At low temperature ($T < 163$ K), the data are consistent with the onset of temperature-independent ^{13}C magnetization transfer via spin diffusion. The temperature dependence of the centers of the rate distributions are fit with $\ln(k_0 e^{-E_a/RT} + k_{SD})$, yielding an apparent activation energy of $E_a = 34 \pm 2$ kJ/mol, a preexponential factor of $k_0 =$

6702 *J. Phys. Chem. A, Vol. 103, No. 34, 1999*

Gédéon et al.

2×10^{10} s^{-1} ($\pm^{1}/_{2}$ decade), and an effective spin diffusion rate coefficient of $k_{SD} = 1.3 \pm 0.2$ s^{-1}. These values represent a convenient parametrization of the complicated benzene dynamics observed by NMR. The apparent activation energy for site-hopping of benzene molecules adsorbed on a faujasite-type zeolite containing Ag^{+} cations is about half of the activation energy observed for benzene adsorbed on a faujasite-type zeolite containing Ca^{2+} cations.[4,7b] In addition, $E_a = 34$ kJ/mol for benzene/Ag$-$Y is comparable to activation energies predicted for benzene adsorbed on Na$-$Y, based on molecular mechanics calculations.[1b,c] While a prefactor of ca. 10^{13} s^{-1} would be expected for a single elementary site-hopping process, the observed parameter $k_0 = 2 \times 10^{10}$ s^{-1} reflects the complicated dynamics of benzene molecules reorienting among multiple local environments in Ag$-$Y zeolite. In conjunction with crystallographic[13,14] and adsorption[54] data, such trends elucidate the effects of cation charge, size, and position on benzene$-$cation interactions in zeolites.

Conclusions

Benzene adsorbed on Ag$-$Y zeolite is a host$-$guest system with a complicated degree of adsorption site disorder. In contrast to more ordered systems, such as benzene adsorbed on Ca$-$LSX or Ca$-$Y zeolites,[4,7] where elementary site-hopping processes have been distinguished and quantified, component site-hopping processes are not resolved for benzene reorientation on Ag$-$Y zeolite. Instead, a distribution of reorientation rates was parametrized using a distribution that was Gaussian on a logarithmic scale, with a fixed width of 1.9 decades and a temperature dependence summarized by the apparent Arrhenius parameters E_a and k_0. In particular, multidimensional exchange ^{13}C NMR techniques and line shape analyses of MAS ^{13}C and static ^{2}H spectra have been used to analyze benzene/Ag$-$Y jump reorientation geometries and dynamics. The benzene reorientation geometry involves a distribution of angles, as shown directly by 2D exchange ^{13}C NMR spectra. A model involving benzene jump motions among tetrahedrally arranged cone caps with 20° opening angles is consistent with the experimental 2D exchange ^{13}C NMR spectra and time-domain echo data. Separate 3D DICO ^{13}C NMR results indicate that the rates of small-angle reorientations are slightly faster than large-angle jump motions. A distribution of molecular reorientation rates is proven by reduced 4D ^{13}C NMR echo measurements, which are consistent with the existence of inequivalent adsorption sites. Exchange processes among different local environments will likely be characterized by different activation energies and preexponential factors. Modeling ^{13}C MAS and static ^{2}H NMR line shapes, combined with 2D exchange and stimulated echo ^{13}C NMR data, yields an apparent activation energy of 34 ± 2 kJ/mol for benzene jumps among adsorption sites in Ag$-$Y zeolite. The apparent activation energy for translational diffusion of benzene within a crystallite of Ag$-$Y zeolite is expected to be similar to this value. These quantitative measurements of molecular reorientation enhance the understanding of the molecular origins of adsorption and transport properties for guest species adsorbed on nanoporous hosts, even in systems with appreciable disorder, such as benzene/Ag$-$Y. Such insights are expected to lead to improved control of zeolite structure and composition variables from which improved separation or reaction properties may be realized.

References and Notes

(1) (a) Bull, L. M.; Henson, N. J.; Cheetham, A. K.; Newsam, J. M.; Heyes, S. J. *J. Phys. Chem.* **1993**, *97*, 11776. (b) Klein, H.; Kirschhock, C.; Fuess, H. *J. Phys. Chem.* **1994**, *98*, 12345. (c) Auerbach, S. M.; Henson, N. J.; Cheetham, A. K.; Metiu, H. I. *J. Phys. Chem.* **1995**, *99*, 10600.

(2) Post, M. F. M. *Stud. Surf. Sci. Catal.* **1991**, *58*, 391.

(3) Heink, W.; Kärger, J.; Pfeifer, H.; Stallmach, F. *J. Am. Chem. Soc.* **1990**, *112*, 2175.

(4) Favre, D. E.; Schaefer, D. J.; Auerbach, S. M.; Chmelka, B. F. *Phys. Rev. Lett.* **1998**, *81*, 5852.

(5) Ruthven, D. M. *Principles of Adsorption and Adsorption Processes*; Wiley: New York, 1984.

(6) (a) Csicsery, S. M. *Zeolites* **1984**, *4*, 202. (b) Venuto, P. B. *Microporous Mater.* **1994**, *2*, 297. (c) Corma, A. *Chem. Rev.* **1995**, *95*, 559.

(7) (a) Wilhelm, M.; Firouzi, A.; Favre, D. E.; Bull, L. M.; Schaefer, D. J.; Chmelka, B. F. *J. Am. Chem. Soc.* **1995**, *117*, 2923. (b) Schaefer, D. J.; Favre, D. E.; Wilhelm, M.; Weigel, S. J.; Chmelka, B. F. *J. Am. Chem. Soc.* **1997**, *119*, 9252.

(8) Larsen, R. G.; Shore, J.; Schmidt-Rohr, K.; Emsley, L.; Long, H.; Pines, A.; Janicke, M.; Chmelka, B. F. *Chem. Phys. Lett.* **1993**, *214*, 220.

(9) Isfort, O.; Boddenberg, B.; Fujara, F.; Grosse, R. *Chem. Phys. Lett.* **1998**, *288*, 71.

(10) Sun, T.; Seff, K. *Chem. Rev.* **1994**, *94*, 857.

(11) (a) Carter, J. L.; Yates, D. J. C.; Lucchesi, P. J.; Elliott, J. J.; Kevorkian, V. *J. Phys. Chem.* **1966**, *70*, 1126. (b) Huang, Y.-Y. *J. Catal.* **1980**, *61*, 461. (c) Muha, G. M. *J. Chem. Phys.* **1971**, *55*, 467.

(12) (a) Gédéon, A.; Burmeister, R.; Grosse, R.; Boddenberg, B.; Fraissard, J. *Chem Phys. Lett.* **1991**, *179*, 191. (b) Grosse, R.; Burmeister, R.; Boddenberg, B.; Gédéon, A.; Fraissard, J. *J. Phys. Chem.* **1991**, *95*, 2443. (c) Grosse, R.; Gédéon, A.; Watermann, J.; Fraissard, J.; Boddenberg, B. *Zeolites* **1992**, *12*, 909.

(13) (a) Fitch, A. N.; Jobic, H.; Renouprez, A. *J. Phys. Chem.* **1986**, *90*, 1311. (b) Yeom, Y. H.; Kim, A. N.; Kim, Y.; Song, S. H.; Seff, K. *J. Phys. Chem. B* **1998**, *102*, 6071.

(14) (a) Gellens, L. R.; Mortier, W. J.; Uytterhoeven, J. B. *Zeolites* **1981**, *1*, 11. (b) Gellens, L. R.; Mortier, W. J.; Uytterhoeven, J. B. *Zeolites* **1981**, *1*, 85.

(15) (a) Baba, T.; Akinaka, N.; Nomura, M.; Ono, Y. *J. Chem. Soc., Faraday Trans.* **1993**, *89*, 595. (b) Cvjeticanin, N. D.; Petranovic, N. A. *Zeolites* **1994**, *14*, 35. (c) Gachard, E.; Belloni, J.; Subramanian, M. A. *J. Mater. Chem.* **1996**, *6*, 867.

(16) Van Dun, J. J. I.; Mortier, W. J.; Uytterhoeven, J. B. *Zeolites* **1985**, *5*, 257.

(17) Bée, M. *Quasielastic Neutron Scattering*; Adam Hilger: Philadelphia, 1988.

(18) (a) Spiess, H. W. *NMR Basic Principles and Progress*; Springer-Verlag: Berlin, 1978; Vol. 15, p 59. (b) Wittebort, R. J.; Olejniczak, E. T.; Griffin, R. G. *J. Chem. Phys.* **1987**, *86*, 5411.

(19) (a) Roduner, E. *Chem. Soc. Rev.* **1993**, *22*, 337. (b) Roduner, E.; Stolmár, M.; Dilger, H.; Reid, I. D. *J. Phys. Chem. A* **1998**, *102*, 7591.

(20) (a) Pfeifer, H. *NMR Basic Principles and Progress*; Springer-Verlag: New York, 1972; Vol. 7, pp 53$-$153. (b) Pfeifer, H. *Phys. Rep. C* **1976**, *26*, 293.

(21) Schmidt-Rohr, K.; Spiess, H. W. *Multidimensional Solid-State NMR and Polymers*; Academic Press: San Diego, 1994.

(22) Benzene 99% ^{13}C-enriched in a single site was purchased from Isotec, 3858 Benner Road, Miamisburg, OH 45342.

(23) (a) Van Greet, A. L. *Anal. Chem.* **1970**, *42*, 679. (b) Kaplan, M. L.; Bovey, F. A.; Cheng, H. N. *Anal. Chem.* **1975**, *47*, 1703.

(24) Ernst, R. R.; Bodenhausen, G.; Wokaun, A. *Principles of Nuclear Magnetic Resonance in One and Two Dimensions*; Clarendon Press: Oxford, U.K., 1987.

(25) (a) Kuebler, S. C.; Heuer, A.; Spiess, H. W. *Macromolecules* **1996**, *29*, 7089. (b) Heuer, A.; Leisen, J.; Kuebler, S. C.; Spiess, H. W. *J. Chem. Phys.* **1996**, *105*, 7088.

(26) Wilhelm, M., Ph.D. Dissertation, Johannes Gutenberg-Universität, Mainz, 1995.

(27) Kaufmann, S.; Wefing, S.; Schaefer, D.; Spiess, H. W. *J. Chem. Phys.* **1990**, *93*, 197−214.

(28) (a) Schmidt, C.; Wefing, S.; Blümich, B.; Spiess, H. W. *Chem. Phys. Lett.* **1986**, *130*, 84. (b) Schmidt, C.; Blümich, B.; Spiess, H. W. *J. Magn. Reson.* **1988**, *79*, 269.

(29) (a) Fujara, F.; Wefing, S.; Spiess, H. W. *J. Chem. Phys.* **1986**, *84*, 4579. (b) Fujara, F.; Wefing, S.; Kuhs, W. F. *J. Chem. Phys.* **1988**, *88*, 6801. (c) Fleisher, G.; Fujara, F. in *NMR Basic Principles and Progress*; Springer-Verlag: Berlin, 1994; Vol. 30, pp 161−207.

(30) Fujara, F.; Geil, B.; Sillescu, H.; Fleischer, G. *Z. Phys. B−Condens. Matter* **1992**, *88*, 195.

(31) Schmidt-Rohr, K.; Spiess, H. W. *Phys. Rev. Lett.* **1991**, 66, 3020.

(32) (a) Heuer, A. *Phys. Rev. E* **1997**, *56*, 730. (b) Kuebler, S. C.; Heuer, A.; Spiess, H. W. *Phys. Rev. E* **1997**, *56*, 741.

(33) Hinze, G.; Böhmer, R.; Diezemann, G.; Sillescu, H. *J. Magn. Reson.* **1998**, *131*, 218.

(34) (a) Pschorn, U.; Rössler, E.; Sillescu, H.; Kaufmann, S.; Schaefer, D.; Spiess, H. W. *Macromolecules* **1991**, *24*, 398. (b) Leisen, J.; Schmidt-Rohr, K.; Spiess, H. W. *J. Non-Cryst. Solids* **1994**, *172−174*, 737.

(35) Lechert, H.; Wittern, K.-P. *Ber. Bunsen-Ges. Phys. Chem.* **1978**, *82*, 1054.

(36) Boddenberg, B.; Burmeister, R. *Zeolites* **1988**, *8*, 488.

(37) Kristenen, J. H.; Bildsøe, H.; Jakobsen, H. J.; Nielsen, N. C. *J. Magn. Reson.* **1992**, *100*, 437.

(38) (a) Schmidt, A.; Vega, S. *J. Chem. Phys.* **1987**, *87*, 6895. (b) Luz, Z.; Poupko, R.; Alexander, S. *J. Chem. Phys.* **1993**, *99*, 7544. (c) Vega, S. *Nuclear Magnetic Resonance Probes of Molecular Dynamics*; Kluwer Academic Publishers: Boston, 1994; pp 155−222.

(39) (a) Wefing, S.; Spiess, H. W. *J. Chem. Phys.* **1988**, *89*, 1219−1233. (b) Wefing, S.; Kaufmann, S.; Spiess, H. W. *J. Chem. Phys.* **1988**, *89*, 1234−1244.

(40) Hagemeyer, A.; Brombacher, L.; Schmidt-Rohr, K.; Spiess, H. W. *Chem. Phys. Lett.* **1990**, *167*, 583.

(41) Auerbach, S. M.; Bull, L. M.; Henson, N. J.; Metiu, H. I.; Cheetham, A. K. *J. Phys. Chem.* **1996**, *100*, 5923.

(42) Saravanan, C.; Auerbach, S. M. *J. Chem. Phys.* **1997**, *107*, 8120.

(43) Jousse, F.; Auerbach, S. M. *J. Chem. Phys.* **1997**, *107*, 9629.

(44) Vitale, G.; Bull, L. M.; Morris, R. E.; Cheetham, A. K.; Toby, B. H.; Coe, C. G.; MacDougall, J. E. *J. Phys. Chem.* **1995**, *99*, 16087.

(45) Favre, D. E.; Schaefer, D. J.; Chmelka, B. F. *J. Magn. Reson.* **1998**, *134*, 261.

(46) Kohlrausch, R. *Pogg. Annal. Phys.* **1854**, *91*, 179.

(47) (a) Williams, G.; Watts, D. C. *Trans. Faraday Soc.* **1970**, *66*, 80. (b) Lindsey, C. P.; Patterson, G. D. *J. Chem. Phys.* **1980**, *73*, 3348.

(48) Dixon, P. K.; Wu, L.; Nagel, S. R.; Williams, B. D.; Carini, J. P. *Phys. Rev. Lett.* **1990**, *65*, 1108.

(49) (a) Resing, H. A. *J. Chem. Phys.* **1965**, *43*, 669. (b) Geil, B.; Fujara, F.; Sillescu, H. *J. Magn. Reson.* **1998**, *130*, 18.

(50) The equation was derived by Heuer and co-workers,[32] assuming that experimental echo intensity is due only to molecules that either have executed correlated back-and-forth jumps or have not reoriented at all. A reorientation geometry involving completely random jumps on the surface of a sphere and effectively infinitely long echo times t_1 through t_4 would be consistent with these assumptions. The presence of a diagonal ridge in 2D exchange ^{13}C NMR spectra in the limit of a long mixing time (see Figure 3b) indicates that these assumptions do not strictly hold in the benzene/Ag−Y system. In such a case, the theoretical $F_{4,cos}(t_{mb})$ curve will be altered slightly and the value in the limit of long t_{mb} may change (Tracht, U. Ph.D. Dissertation, Johannes Gutenberg-Universität, Mainz, 1998). Although the equation may not be strictly applicable to the benzene/Ag−Y system, it provides a reasonable fit to the 4D echo data within experimental resolution.

(51) (a) Auerbach, S. M.; Metiu, H. I. *J. Chem. Phys.* **1997**, *106*, 2893. (b) Saravanan, C.; Auerbach, S. M. *J. Chem. Phys.* **1997**, *107*, 8132. (c) Saravanan, C.; Jousse, F.; Auerbach, S. M. *J. Chem. Phys.* **1998**, *108*, 2162.

(52) To keep the model used in the MAS simulations simple, the overall rates of small- and large-angle reorientation processes from each of the 12 sites were set equal. Although this model assumption is not entirely consistent with the DICO results shown in Figure 7, which indicate that small-angle reorientations are faster than large-angle jump motions, the changes in the simulated MAS spectra obtained by setting the rate of small-angle reorientation to twice that of the large-angle reorientation rate are minuscule.

(53) Favre, D. E. Ph.D. Dissertation, University of California, Santa Barbara, 1999.

(54) Blank, H.; Bülow, M.; Schirmer, W. *Z. Phys. Chem.* **1979**, *260*, 395.